

GT2011-46036

CFD OPTIMIZATION OF GAS-SIDE FLOW CHANNEL CONFIGURATION INSIDE A HIGH TEMPERATURE BAYONET TUBE HEAT EXCHANGER WITH INNER AND OUTER FINS

T. Ma Y.P. Ji M. Zeng Q.W. Wang*

Key Laboratory of Thermal Fluid Science and Engineering of MOE
Xi'an Jiaotong University, Xi'an, Shaanxi, 710049, P.R. China

ABSTRACT

In this paper, the gas-side fluid flow distribution inside a bayonet tube heat exchanger with inner and outer fins is numerically studied. The heat exchanger is designed based on the traditional bayonet tube heat exchanger, where compact continuous plain fins and wave-like fins are mounted on the outside and inside surfaces of outer tubes, respectively, to enhance the heat transfer performance. However, gross flow maldistribution and large vortices are observed in the gas-side flow channel of baseline design. In order to improve the flow uniformity, three modified designs are proposed. Three vertical plates and two inclined plates are mounted on the inlet manifold for Model B. For the Model C, another six bending plates are mounted on the middle manifolds and three pairs of them are connected together. The Model D has a similar structure as Model C except for the two additional baffles. The results indicate that the flow distributions of Model C and D are much more uniform under different inlet Reynolds number, especially in the high inlet Reynolds number. Although the flow distribution of Model D is the best, its pressure drop is 2.6 times higher than that of Model C. Therefore, the design of Model C is the most optimized structure. Compared with the original design, the nonuniformity of Model C can be reduced by 42% while the pressure drop is almost the same under the baseline condition. [**Keywords:** bayonet tube heat exchanger; plain finned tube; flow distribution; pressure drop; nonuniformity]

INTRODUCTION

High temperature heat exchangers (HTHEs) are urgently needed in the hydrogen producing sulfur-iodine (S-I) thermochemical cycle, the very high temperature reactor (VHTR) and the externally fired combined cycle (EFCC). Different concepts of HTHEs were investigated such as Ref. [1-5]. In order to improve the heat transfer performance and reduce the cost, a bayonet tube heat exchanger with fins employed

outside and inside outer tubes of bayonet elements was proposed in previous research [6-8]. However, crude flow maldistribution in the gas side was found during the design process. In fact, the problem of flow maldistribution maybe decrease the heat transfer performance and increase the pumping power. It has been recognized and investigated by numerous researchers. Ponyavin and Chen et al. [9] analyzed the flow distribution inside a compact ceramic high temperature heat exchanger and chemical decomposer by numerical method. The results indicated that the flow maldistribution in baseline design heat exchanger was very serious. Then they proposed several improved designs of manifolds and supply channels, which could sufficiently enhance the uniformity of the flow rate distribution as well as an appropriate pressure drop. Zhang [10] conducted experimental and numerical simulation investigations on an air to air plate-fin heat exchanger. The study indicated that the channel pitch was one of the crucial factors that influenced the flow maldistribution. When the channel pitch was larger than 2 mm, the maldistribution was serious and the thermal effectiveness was deteriorated by 10-20%. Ismail and Ranganayakulu et al. [11] presented a numerical investigation of three typical compact plate-fin heat exchangers to analyze the flow maldistribution effects with ideal and real cases. The headers had been modified by providing suitable baffle plates for the improvement of flow distribution. Nie and Chen et al. [12] studied the pressure and velocity distributions in the bipolar plate of a proton exchange membrane (PEM) electrolysis cell. It was shown that both the velocity and temperature distributions in the channels were very non-uniform over the test plate and reverse flow existed in the exit tube and near the connection between the exit tube and channels. Further, numerical simulations on the two-phase water/oxygen flow in the bipolar were also conducted by Nie and Chen et al. [13]. It demonstrated that the reverse flow developed inside the flow channels with the increase of mass flow rate of oxygen generation and there existed a significant difference between single-phase flow cases and two-phase flow cases. Zhang and

Wen et al. [14, 15] proposed two modified headers with a two-stage-distributing structure for the inlet configuration of plate-fin heat exchangers. The numerical and experimental results indicated that the improved header could effectively enhance the uniformity of flow distribution and efficiency compared with conventional headers used in industry. Zhang and Wang et al. [16] studied the flow performance of gas cavity configuration of the recuperator in a 100kW microturbine system. The best gas cavity configuration might greatly decrease the velocity nonuniformity by 73.3% while the corresponding pressure drop increased by 8% comparing with the worst one. Qu and Gao [17] investigated the flow distribution and pressure loss in the air induct structure for microturbine recuperator. The results showed that the non-distribution of the optimized structure could be decreased from 67% to 13%, while the pressure loss could be decreased by 50% compared with the base line design. It can be seen that the flow maldistribution has an important effect on the heat transfer and pressure drop performances and should be paid more attention. Further, many researchers [10, 15] have recognized that the thermal performance will be deteriorated by the flow maldistribution according to their study. Therefore, the flow uniformity is widely considered as a direct indicator for the structure optimization [9-17].

The present paper mainly investigates the gas-side flow distribution inside a bayonet tube heat exchanger with inner and outer fins by CFD method and optimizes its configuration.

NOMENCLATURE

c_p	Specific heat at constant pressure, J/(kg·K)
c_2	Inertial resistance factor, m^{-1}
d_h	Equivalent diameter, m
D_o	Outer diameter of outer tube, m
f	Darcy friction factor
F_p	Outer fin pitch, m
k	Kinetic energy of turbulence, $m^2 \cdot s^{-2}$
L	Tube length, m
N	Channel numbers
N_t	Number of tube rows
p	Static pressure, Pa
P_t	Transverse tube pitch, m
P_l	Longitudinal tube pitch, m
$q_{m,i}$	Mass flow rate of channel, kg/s

\bar{q}_m	Average mass flow rate, kg/s
Re	Reynolds number
S	Average nonuniformity of mass flow rate
S_ϕ	Source term
\bar{v}_D	Frontal velocity, m/s
\bar{v}_i	True velocity, m/s
x_i	Coordinate, m

Greek

δ	Fin thickness, m
ρ	Density, kg/m^3
μ	Dynamic viscosity, $kg/(m \cdot s)$
ϕ	Generalized variable
ε	Dissipation rate of kinetic energy of turbulence, $m^2 \cdot s^{-3}$
Γ_ϕ	Diffusion coefficient
Δp	Pressure drop between inlet and outlet, Pa
∂	Permeability, m^2
σ	Contraction ratio of plain finned tubes

BAYONET TUBE HIGH TEMPERATURE HEAT EXCHANGER WITH INNER AND OUTER FINS

The designed bayonet tube heat exchanger is shown in Fig.1. In order to enhance the heat transfer performance, fins are welded outside and inside outer tubes of the bayonet elements. This HTHE is especially suitable for gas to gas high temperature heat exchangers due to their low heat transfer performance on both sides. Various fins such as circular fins, continuous plain fins, strip fins, slit fins and louver fins can be mounted on the outside surfaces of outer tubes. Longitudinal plain fins and wave-like fins can be employed on the inside surfaces of outer tubes. More detailed descriptions are shown in Ref. [6-8].

The cold air enters from the lower inlet port. Then it flows along the annulus and inner tubes of the bayonet elements of the 3rd zone by turns. When it arrives at the 1st zone, it flows back into the bayonet elements of the 2nd zone. It exits from the upper outlet port in the end. The hot gas flows in the shell side. The hot gas flows in the 2nd zone of the shell side at first and then it flows in the 3rd zone of the shell side. This paper analyzes the flow distribution of the shell side. Due to the geometrical symmetry, the domain of the 2nd zone is selected as the computational domain.

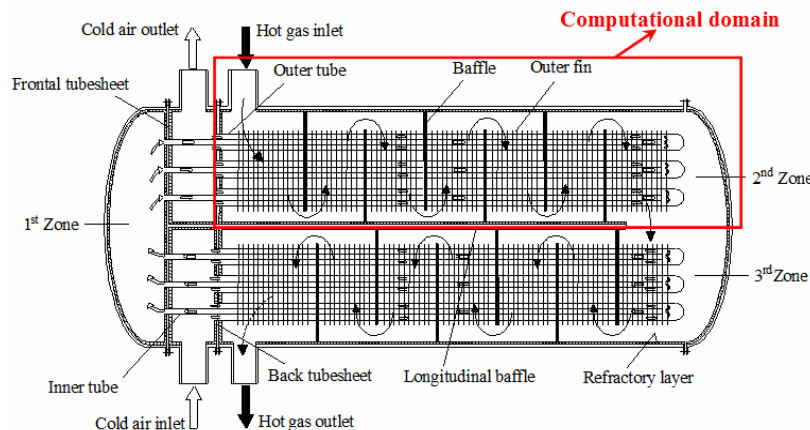


Fig.1 Sketch of bayonet tube HTHE with inner and outer fins

PHYSICAL MODEL

In the present study, the computational domain is simplified to a two dimensional (2D) model because there are a lot of tubes vertical to the plane. The geometry of the baseline design is shown in Fig. 2(a). It consists of plain finned tubes, two baffles, one inlet duct, one outlet duct and corresponding manifolds. It should be noted that one channel is composed of two adjacent fins and their fluid flow channel. The domain of the plain finned tubes includes 180 channels, while the number of channels between adjacent baffles is 60. The diameters of inlet and outlet ducts are 0.1m. The height and pitch of baffles are 0.26m and 0.18m, respectively. Table 1 shows the geometrical parameters of the plain finned tubes.

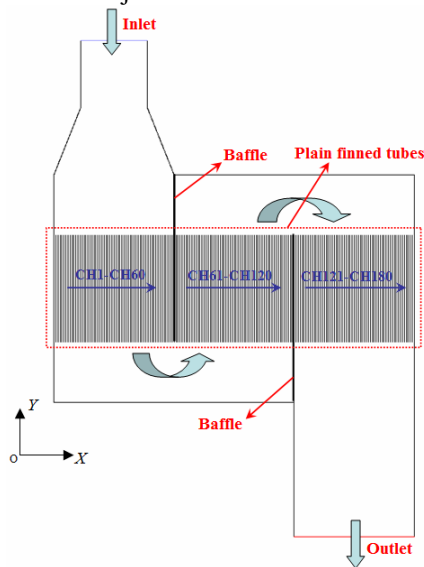
Table 1 Geometrical parameters of plain finned tubes

Variables	Present model	Validation model
Outer diameter of outer tube (D_o , m)	0.028	0.01015
Transverse tube pitch (P_t , m)	0.046	0.025
Longitudinal tube pitch (P_l , m)	0.04	0.02165
Number of tube rows (N_t)	4	4
Outer fin pitch (F_p , m)	0.003	0.002
Fin thickness (δ , m)	0.25×10^{-3}	0.2×10^{-3}
Tube length (L , m)	0.54	0.04

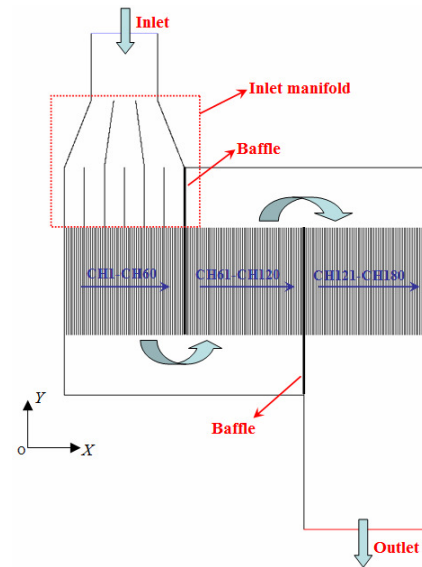
Figures 2(b)-(d) show the three modified design models, respectively. The Model B has the same dimension as Model A with the exception of inlet manifold. The new inlet manifold has three vertical plates and two inclined plates, which are equidistantly located along the direction of X-coordinate.

The Model C is modified based on Model B. It adds six bending plates near the outlet and inlet of the channels in the middle manifolds. They are also equidistantly located along the direction of X-coordinate. Furthermore, three pairs of them are connected together for the purpose of guiding the fluid flow. The shape of bending plate is one quarter of the ellipse, whose long axis is two times longer than short axis.

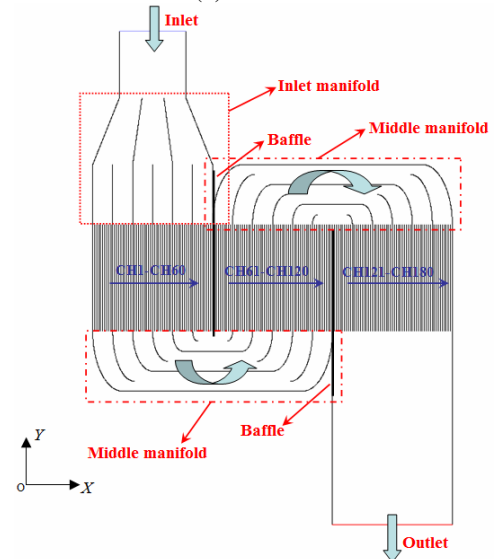
The Model D has a similar basic structure as Model C. However, two additional baffles are mounted so that the number of channels between adjacent baffles is reduced to 36.



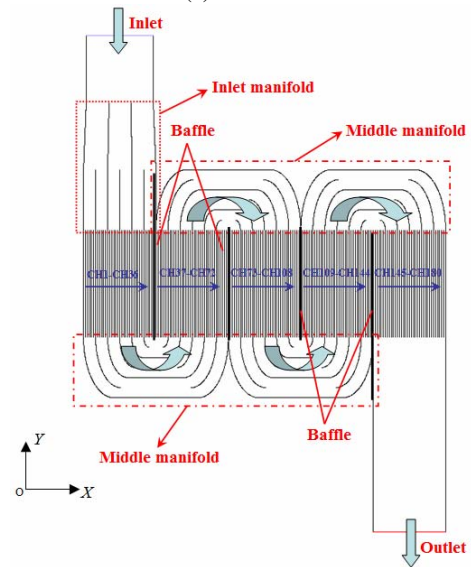
(a) Model A



(b) Model B



(c) Model C



(d) Model D

Fig.2 Sketch of four different design models

NUMERICAL METHODS

The RNG $k-\varepsilon$ model is suitable for predicting the turbulent vortex flow. There exist evident turbulent vortexes caused by the tubes in the plain finned tube cell. According to the comparison of different models on the fin and tube heat exchangers by Tian et al. [18], the numerical results indicated that it had better agreements with the experimental data than other models. Therefore, the RNG $k-\varepsilon$ model with wall function method is also adopted for the present simulation. The general governing equations can be expressed as follows:

$$\text{div}(\rho \vec{V} \phi) = \text{div}(\Gamma_{\phi} \text{grad} \phi) + S_{\phi} \quad (1)$$

where, ϕ is the generalized variable which represents the velocity \vec{V} , the kinetic energy of turbulence k and the dissipation rate of the kinetic energy of turbulence ε in different solved equations. Γ_{ϕ} and S_{ϕ} are the appropriate diffusion coefficient and source term for each variable ϕ . More details can be found in Ref. [18].

For the inlet boundary condition, uniform inlet velocity is used. The pressure-out is applied to the outflow boundary. Due to the large numbers of fins and tubes, it is impossible to study the whole plain finned tubes domain using the traditional model. The porous media model has been applied to simulate the plate-fin core of plate-fin heat exchanger [10-11], wave plates of recuperator for microturbine [17], elliptic tube banks of recuperative heat exchangers for an aero engine [19], core blocks of reactor vessel [20], and so on. Every channel of the plain finned tubes is considered as a porous media in the present study. For the baffles, guiding plates, fins and outside walls, no-slip conditions are used. The gas flowing in the model is hot dry air. The properties of air are given as follows: for 1273K, $\rho_{\text{air}}=0.277 \text{ kg/m}^3$, $\mu_{\text{air}}=4.9 \times 10^{-5} \text{ kg/(m}\cdot\text{s)}$; for 303K, $\rho_{\text{air}}=1.165 \text{ kg/m}^3$, $\mu_{\text{air}}=1.86 \times 10^{-5} \text{ kg/(m}\cdot\text{s)}$.

The Forchheimer–Brinkman extended Darcy model [21] is adopted to simulate the fluid flow in the porous media, which is composed of the inertia and viscosity terms. Accordingly, additional source term is applied to the momentum equations in FLUENT which are given by:

$$S_i = -\frac{dp}{dx_i} = \frac{\mu}{\phi} \bar{v}_i + c'_2 \frac{1}{2} \rho |\bar{v}_i| \bar{v}_i \quad (2)$$

where, \bar{v}_i is the true velocity of the porous media and can be calculated by:

$$\bar{v}_i = \frac{\bar{v}_D}{\phi} \quad (3)$$

In the plain finned tubes, the pressure drop is usually determined by:

$$\frac{\Delta p}{\Delta x_i} = f \cdot \frac{1}{2} \rho \left(\frac{\bar{v}_D}{\sigma} \right)^2 \frac{1}{d_h} \quad (4)$$

$$f = \frac{c_1}{Re} + c_2 \quad (5)$$

$$Re = \frac{\rho (|\bar{v}_D| / \sigma) d_h}{\mu} \quad (6)$$

where, d_h is the equivalent diameter, which refers to tube diameter in the plain finned tubes. The f is Darcy friction factor.

It can be obtained from experiment or numerical simulation. According to the previous study of the plain finned tube cells, the parameter values of Eq. (5) are given as follows: for 1273K, $c_1=3938$, $c_2=0.55813$; for 303K, $c_1=7492$, $c_2=0.29805$.

According to Eqs. (2)-(6), the permeability ∂ and inertial resistance factor c'_2 of the main flow direction (Y) can be calculated by Eqs.(7) and (8). Since the fluid mainly flows in the Y direction, the permeability and inertial resistance factor in the X direction are set to infinitely big.

$$\partial = \frac{d_h^2 \cdot \sigma}{c_1 / 2 \cdot \phi} \quad (7)$$

$$c'_2 = \frac{\phi^2 \cdot c_2}{\sigma^2 \cdot d_h} \quad (8)$$

The commercial software FLUENT6.2 is selected as the tool for the study. The software solves the governing equations by a finite control volume method. Semi-implicit method for pressure linked equations (SIMPLE) algorithm is used to deal with the coupling between pressure and velocity fields. The convection terms are handled by the power-law difference scheme. The criterions of convergence are that the residual for every variable should be less than 10^{-5} .

GRID INDEPENDENCE AND CODE VALIDATION

In order to ensure the independence of grid number on the results, five kinds of grid systems have been established and compared at a representative condition. As is shown in Fig.3, the difference is not evident when the nodes numbers are greater than 1.0×10^6 . The maximum relative deviation (G4 is assumed as the base line) is less than 1%. To save the computer resource and computational time, G4 is selected as the grid system in the later calculations.

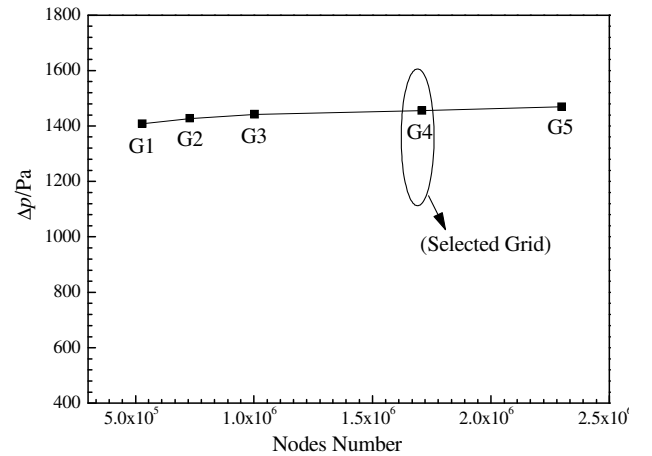


Fig.3 Grid independence test

Because the tube diameter is larger than the traditional tube diameter in industrial plain finned tubes, a similar plain finned tube cell is modeled at first to obtain its friction factor. Its geometrical parameters are shown in Table 1. Then a similar 2D porous media model of plain finned tubes in a straight channel is established and the same numerical method is used to investigate the pressure drop performance of plain finned tubes, as shown in Fig.4. The numerical results are described in Fig.5.

Compared to the correlation established by Wang et al. [22], the maximum deviation is 19%, while the average deviation is 11%.

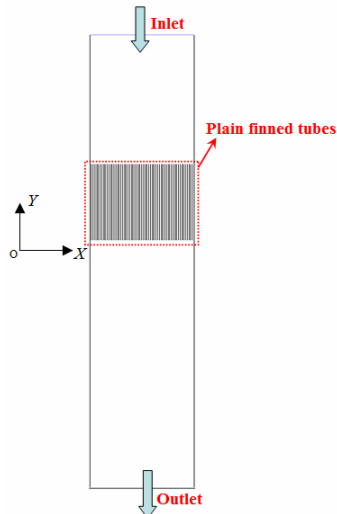


Fig.4 Model of plain finned tubes in a straight channel

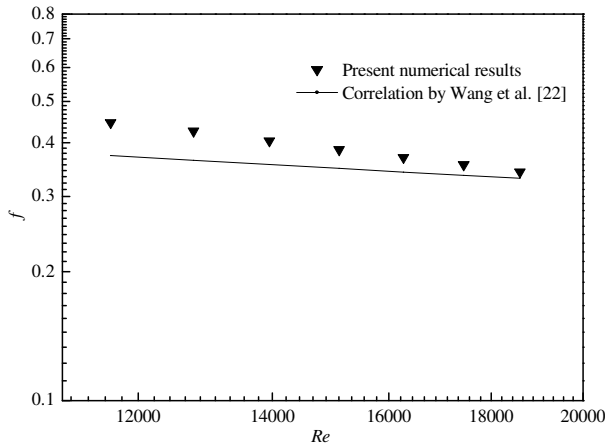
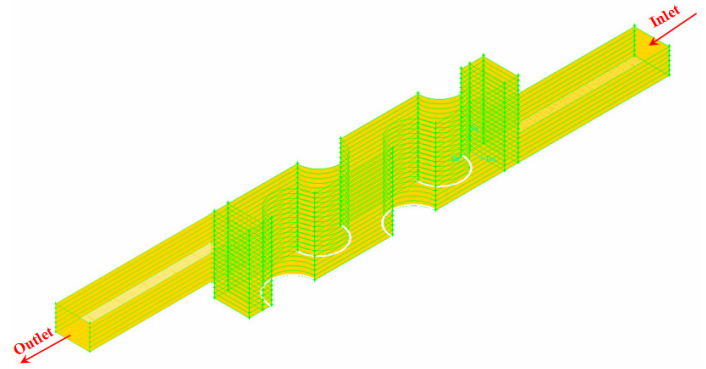
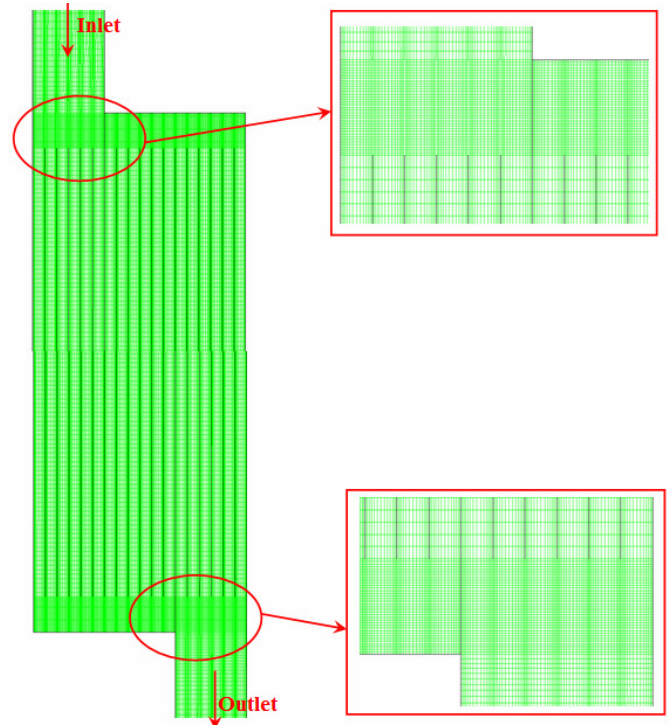


Fig.5 Validation of plain finned tubes in a straight channel

In order to further validate the local characteristics of the porous media method, a detailed full-sized 3D model with 18 channels is established, as shown in Fig.6(a). The corresponding 2D porous media model is also accomplished, as shown in Fig.6(b). The mesh grids in the middle manifolds and nearby the fins are refined. This kind of mesh grids is exactly the same as the grid system G4 discussed above. The validation structure is similar to Model A except for the channel numbers. They are compared under identical inlet mass flow rate. One of the representative results under inlet mass flow rate of 0.4 kg/s is shown in Fig.7. It can be seen that the fluid flow distributions of the two models are very similar. Meanwhile, the pressure drop for the 3D and 2D models is 12.6 kPa and 11.3kPa, respectively. The good agreement validates the reliability of the physical model and numerical codes. However, the required nodes number is 4.859 million for the 3D model, while 0.067 million for the 2D model. It is impossible to simulate the total model with 180 channels because the common personal computer is hard to afford such a big nodes number. And longer computational time is also required. Therefore, the porous media method is a suitable method to save computer resource and computational time for the engineering applications.



(a) Full-sized 3D model with 18 channels



(b) 2D porous media model with 18 channels

Fig.6 3D and 2D models with 18 channels for validation

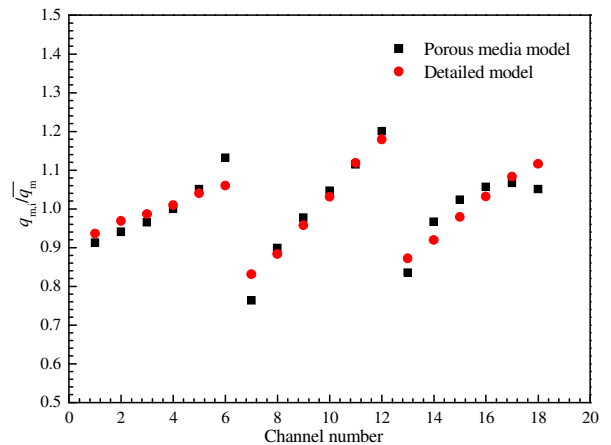


Fig.7 Comparison of porous media and detailed models

RESULTS AND DISCUSSION

In the real operating condition, there exists a significant temperature decrease along the main flow direction as well as a great variation of fluid properties such as dynamic viscosity, density and thermal conductivity. The present study only focuses on the flow performance, but the heat transfer performance is not considered. The mass flow distributions of Model A under different temperature conditions are compared, as shown in Fig.8. The temperature and fluid properties are kept as constant in each temperature condition. It can be seen that all the variation trends are almost the same. The worst mass flow distribution occurs in the lowest temperature condition because the flow distribution is mainly affected by the back pressure drop and the pressure drop in this condition is the lowest. Therefore, the lowest temperature condition can be considered as the representative condition and adopted in the later calculations.

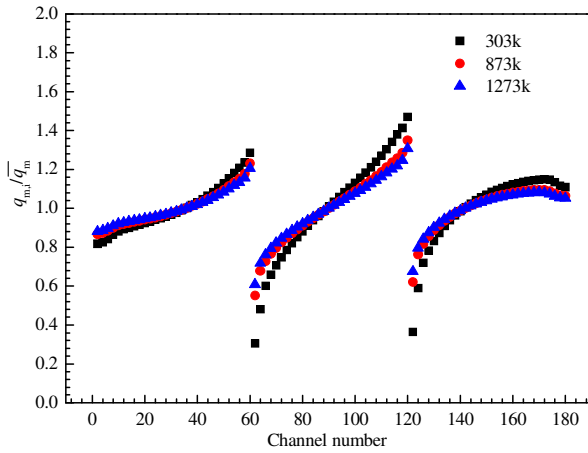
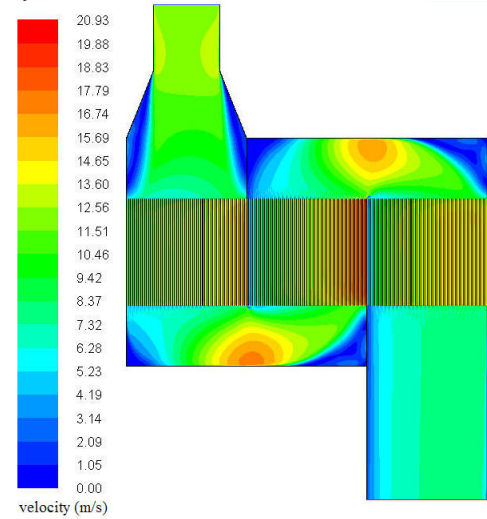


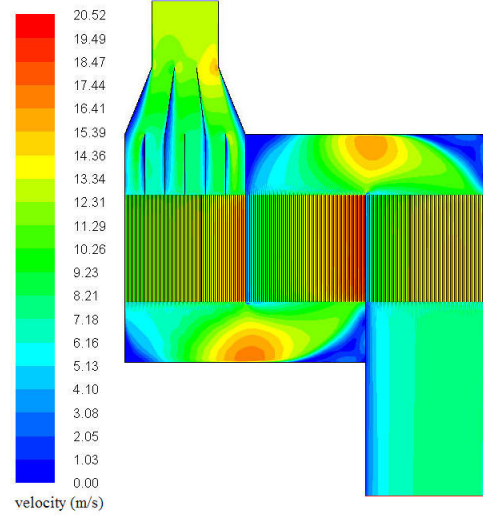
Fig.8 Mass flow distributions of Model A under different temperatures

The four design models have been investigated when the inlet Reynolds number is kept as 77792. It should be noted that the equivalent diameter of inlet Reynolds number discussed later refers to the diameter of inlet duct. The velocity distributions are shown in Fig.9. As can be seen in Fig.9 (a), the velocity distributions are very non-uniform, especially in the middle manifolds. Among every group of channels (1# channels: CH1-CH60, 2# channels: CH61-CH120 or 3# channels: CH121-CH180), the velocity becomes bigger and bigger from the left side to the right side, which means that larger mass flow rates pass through the right-side channels. The reason is that the major fluids accumulate in the right side before entering into the channels and then flow into the channels directly. In addition, large vortices are observed in the corners of middle manifolds and inlet manifold. In Fig.9 (b), it can be seen that the flow distribution in the inlet manifold and group 1 of channels is a little more uniform than that of Model A. However, the big maldistribution occurs after the plain finned tubes domain and the flow distribution is almost the same in the later flow channels. In order to deal with the problems, some bending plates are proposed to be mounted in the middle manifolds, as shown in Fig.9 (c). They have an important effect on the flow distribution. Only small vortices are produced near the inlet of plain finned tubes and a few fluids accumulate in the connection plates. Theoretically more bending plates can achieve more uniform flow distribution, but it may also

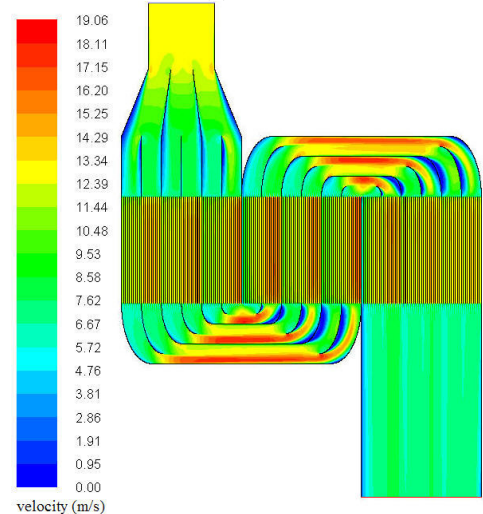
complicate the manufacture. For Model D, the flow distribution is much more uniform than that of Model C due to the increased baffles. And the obvious vortices are disappeared. However, the velocity in the plain finned tubes, inlet baffle and middle baffles dramatically increases.



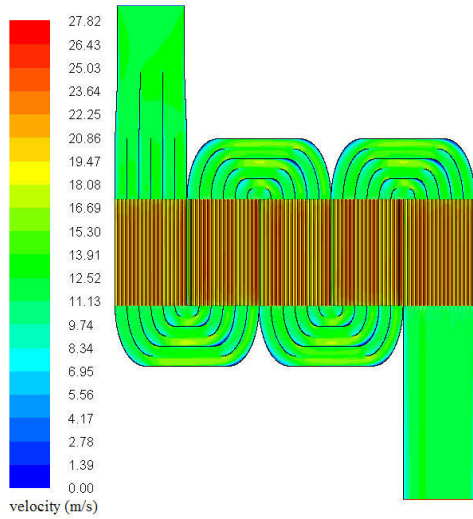
(a) Model A



(b) Model B



(c) Model C

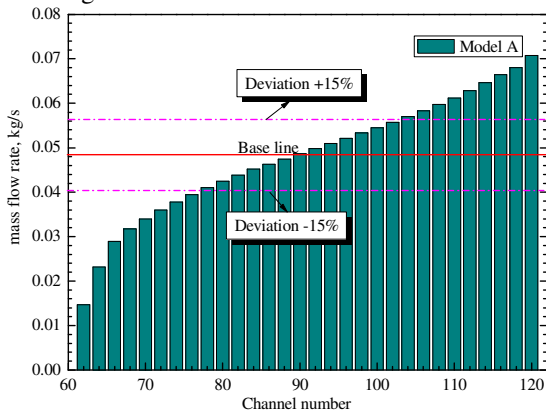


(d) Model D

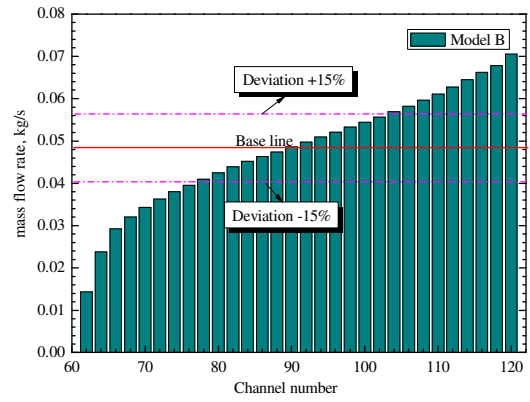
Fig.9 Velocity distributions

Figure 10 plots the mass flow distributions of the 2# channels in details. Due to the large numbers of channels, the mean mass flow rate of adjacent two channels from the left side to the right side is shown in the Fig.10 for the purpose of describing it more clearly. The mass flow rates for the Model A and B become larger and larger from the left-side channels to the right-side channels. More than half of the channels are under severe maldistribution with the deviations of mass flow rates in excess of 15%. The slopes of their growth are almost the same. Hence, only the modified inlet manifold is not enough to improve the flow performance. However, the mass flow rates for the Model C and D vary in wave shape rather than sharp inclined lines. The peak mass flow rates are much smaller compared with the Model A and B. Most of the deviations of mass flow rates are less than 15%. The flow performance of Model D is the best among the four models.

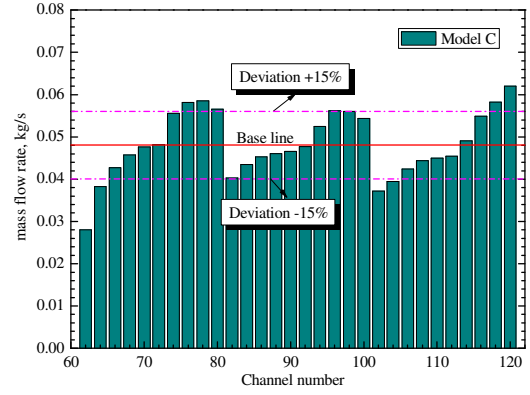
The pressure distributions are shown in Fig.11. The overall pressure drop for Model A is 1.455 kPa, Model B 1.456 kPa, Model C 1.424 kPa, and Model D 5.2 kPa. The pressure drop mainly takes place in the plain finned tubes domain so that the pressure drop for the Model A, B and C is almost the same. Therefore, the additional guiding plates have little effect on the pressure loss. The pressure distributions of the middle manifolds for the Model C and D are much more uniform compared with that for Model A and B. However, the pressure drop of Model D is 2.6 times higher than that of Model C.



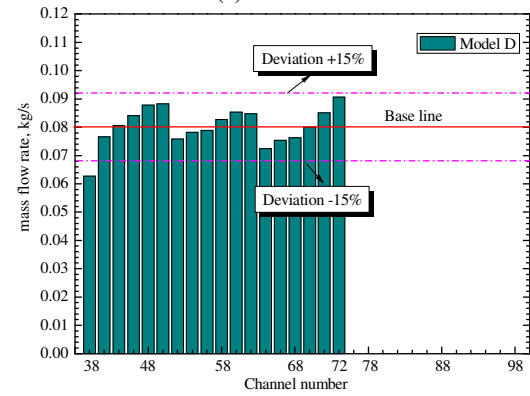
(a) Model A



(b) Model B

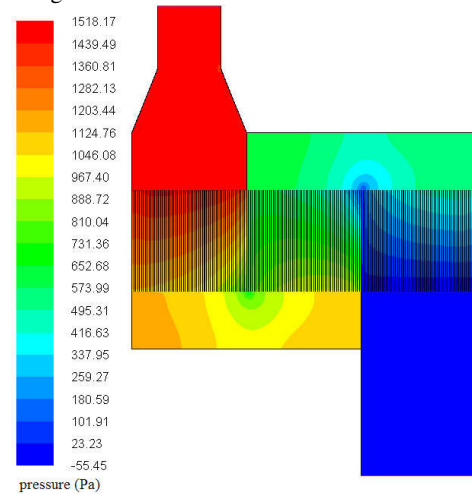


(c) Model C

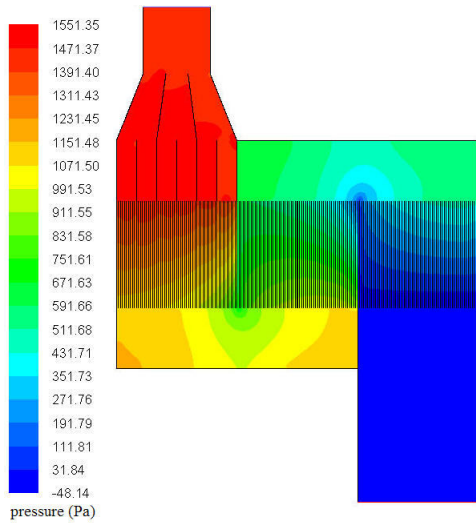


(d) Model D

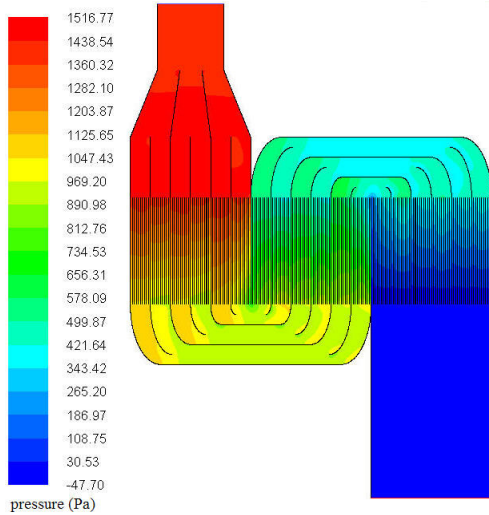
Fig.10 Mass flow distributions of 2# channels



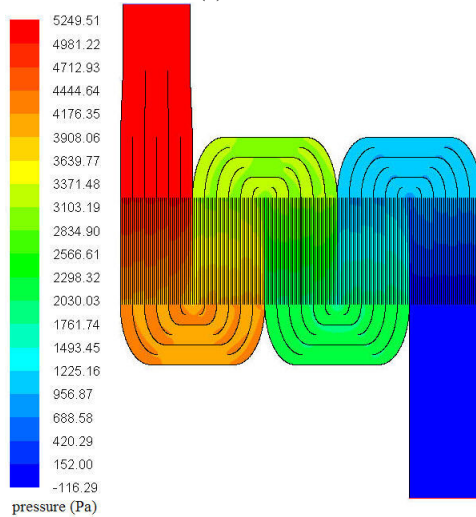
(a) Model A



(b) Model B



(c) Model C



(d) Model D

Fig.11 Pressure distributions

The average nonuniformity of mass flow rate S is used for the quantitative analysis of flow maldistribution, which is defined as:

$$S = \frac{\sqrt{\sum_{i=1}^N (q_{m,i} - \bar{q}_m)^2 / (N-1)}}{\bar{q}_m} \quad (9)$$

The average nonuniformity of mass flow rate for the four models under different inlet Reynolds number is shown in Fig.12. It indicates that the nonuniformity increases with increasing the inlet Reynolds number. The nonuniformity of Model A and B is much bigger than that of Model C and D. Moreover, the increased declination trend of Model A and B is the biggest. It can be concluded that the Model C and D is superior to other models, especially in the high inlet Reynolds number conditions. The corresponding pressure drop is shown in Fig.13. The pressure drops of the four models increase with the increase of inlet Reynolds number. However, the pressure drop is too high that the Model D is unsuitable for the heat exchanger. Compared with the Model A, the nonuniformity of Model C can be reduced by 42% while the pressure drop is almost the same under the baseline condition.

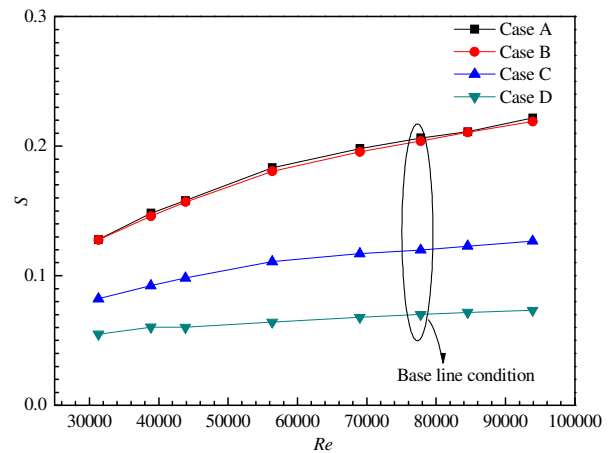


Fig.12 Nonuniformity of mass flow rate vs. inlet Reynolds number

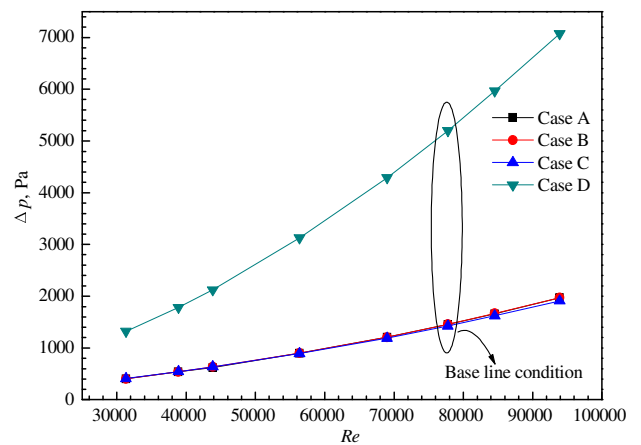


Fig.13 Pressure drops vs. inlet Reynolds number

CONCLUSIONS

In this paper, the gas-side fluid flow distribution inside a bayonet tube heat exchanger with inner and outer fins has been investigated by CFD method. The porous media model is applied to simulate the plain finned tubes. The velocity distributions of the baseline design are very non-uniform,

especially in the middle manifolds. And large vortices are observed in the corners of middle manifolds and inlet manifold. Due to the big maldistribution in the middle manifolds, the mass flow rates become larger and larger from the left-side channels to the right-side channels in every group of channels.

For the purpose of improving the flow performance, three modified designs are proposed. The Model B adds three vertical plates and two inclined plates to the inlet manifold. But it has little improvement on the flow distribution with the exception of the flow in the inlet manifold and the first group of channel. Then six bending plates (Model C and D) are mounted on the middle manifolds and three pairs of them are connected together for the purpose of guiding the fluid flow. The peak mass flow rates are much smaller compared with Model A and B. Most of the deviations of mass flow rates in the second group of channels are less than 15%. The flow distributions of Model C and D are much more uniform under different Reynolds number, especially in high inlet Reynolds number. The flow distribution of Model D is the best due to the added baffles. However, the pressure drop of Model D is 2.6 times higher than that of Model C, which is unsuitable for the present heat exchanger. Therefore, the design of Model C is the most optimized structure. Compared with the original design, the nonuniformity of Model C can be reduced by 42% while the pressure drop is almost the same under the baseline condition.

ACKNOWLEDGMENTS

This work is supported by the National High Technology R&D Project of China (No. 2007AA05Z204), the International Cooperation Program of Science and Technology R&D Project of Shaanxi Province (No. 2006KW-24) and the Fundamental Research Funds for the Central Universities.

REFERENCES

- [1] Ponyavin V., Chen Y.T., Hechanova A.E., Wilson M., Numerical modeling of compact high temperature heat exchanger and chemical decomposer for hydrogen production, *Heat Mass Transfer*, 2008, 44:1379-1389
- [2] De Losier C.R., Subramanian S., Ponyavin V., Chen Y.D., Hechanova A.E., Peterson P.F., The parametric study of an innovative offset strip-fin heat exchanger, *Journal of heat transfer-transactions of the ASME*, 2007, 129:1453-1458
- [3] Mylavarapu S., Sun X.D., Figley J., Needler N., Christensen R., Investigation of High Temperature Printed Circuit Heat Exchangers for Very High Temperature Reactors, *Journal of Engineering for Gas Turbines and Power*, 2009, 131:062905
- [4] Schulte-Fischedick J., Dreissigacker V., Tamme R., An innovative ceramic high temperature plate-fin heat exchanger for EFCC processes, *Applied Thermal Engineering*, 2007, 27:1285-1294
- [5] O'Doherty T., Jolly A.J., Bates C.J., Optimisation of heat transfer enhancement devices in a bayonet tube heat exchanger, *Applied Thermal Engineering*, 2001, 21:19-36
- [6] Wang Q.W., Ma T., Chen Q.Y., Internal and external fins intubations type high temperature heat exchanger, Chinese Patent, 2010, ZL200810150820.3 (In Chinese)
- [7] Ma T., Xie G.N., Wang Q.W., Thermal design of a high temperature bayonet tube heat exchanger with inner and outer fins, *ASME Turbo Expo 2009: Power for Land, Sea and Air*, June 8-12, 2009, Orlando, FL, USA, GT2009-60283
- [8] Ma T., Lin M., Zeng M., Ji Y.P., Wang Q.W., Numerical Study of Internally Finned Bayonet Tubes in a High Temperature Bayonet Tube Heat Exchanger with Inner and Outer Fins, *ASME Turbo Expo 2010: Power for Land, Sea and Air*, June 14-18, 2010, Glasgow, Scotland, UK, GT2010-22360
- [9] Ponyavin V., Chen Y.T., Cutts J., Wilson M., Hechanova A.E., Calculation of fluid flow distribution inside a compact ceramic high temperature heat exchanger and chemical decomposer, *Journal of fluids engineering-transactions of the asme*, 2008, 130(6):061104
- [10] Zhang L.Z., Flow maldistribution and thermal performance deterioration in a cross-flow air to air heat exchanger with plate-fin cores, *International journal of heat and mass transfer*, 2009, 52(19-20): 4500-4509
- [11] Ismail L.S., Ranganayakulu C., Shah R.K., Numerical study of flow patterns of compact plate-fin heat exchangers and generation of design data for offset and wavy fins, *International journal of heat and mass transfer*, 2009, 52(17-18): 3972-3983
- [12] Nie J.H., Chen Y.T., Cohen S., Carter B.D., Boehm R.F., Numerical and experimental study of three-dimensional fluid flow in the bipolar plate of a PEM electrolysis cell, *International journal of thermal sciences*, 2009, 48:1914-1922
- [13] Nie J.H., Chen Y.T., Numerical modeling of three-dimensional two-phase gas-liquid flow in the flow field plate of a PEM electrolysis cell, *International Journal of Hydrogen Energy*, 2010, 35(8):3183-3197
- [14] Zhang Z., Li Y.Z., CFD simulation on inlet configuration of plate-fin heat exchangers, *Cryogenics*, 2003, 43, (12):673-678
- [15] Wen J., Li Y.Z., Zhou A.M., Zhang K., An experimental and numerical investigation of flow patterns in the entrance of plate-fin heat exchanger, *International Journal of Heat and Mass Transfer*, 2006, 49, (9-10):1667-1678
- [16] Zhang D.J., Wang Q.W., Zeng M., Luo L.Q., Wu F., Feng Z.P., CFD optimization of gas inlet configuration for 100kw microturbine recuperator, *Proceeding of GT2006 ASME Turbo Expo 2006: Power for Land, Sea and Air*, May 8-11, 2006, Barcelona, Spain, GT2006-90256
- [17] Qu W., Gao S., Effects of air inlet structure to flow uniformity and resistance for primary surface recuperator of a micro gas turbine, *Proceeding of the 14th international heat transfer conference, IHTC14*, August 8-13, 2010, Washington, DC, USA, IHTC14-22332
- [18] Tian L.T., He Y.L., Tao Y.B., Tao W.Q., A comparative study on the air-side performance of wavy fin-and-tube heat exchanger with punched delta winglets in staggered and in-line arrangements, *International journal of thermal sciences*, 2009, 48(9):1765-1776
- [19] Missirlis D., Yakinthos K., Palikaras A., Katheder K., Goulas A., Experimental and numerical investigation of the flow field through a heat exchanger for aero-engine applications, *International Journal of Heat and Fluid Flow*, 2005, 26(3):440-458
- [20] Oh C.H., Kim E.S., Air ingress analysis: computational fluid dynamic models, *Proceeding of the 14th international heat transfer conference, IHTC14*, August 8-13, 2010, Washington, DC, USA, IHTC14-23083
- [21] Nield D.A., Bejan A., *Convection in Porous Media*, 3rd ed., Springer, New York, 2006
- [22] Wang C.C., Chi K.Y., Chang C.J., Heat transfer and friction characteristics of plain fin-and-tube heat exchangers. II. Correlation, *International Journal of Heat and Mass Transfer*, 2000, 43(15):2693-700